ADVANCED MATERIALS
www.advmat.de

Counterintuitive Fluorescence Blue Shift in Symmetry Breaking Dicationic Bis(indolium) with Two-Photon Absorption Properties for NIR Living Cell Imaging

Carlos Benitez-Martin, Jose M. Marin-Beloqui, Juan T. López Navarrete, Juan Casado, Francisco Najera,* and Ezequiel Perez-Inestrosa**

Two-photon absorption (2PA) has become a cornerstone for bioimaging, enabling deeper tissue penetration while minimizing photodamage. Recently, the correlation between 2PA and excited-state symmetry breaking (ES-SB) has been probed. Typically, the first hallmark of ES-SB is a red shift in fluorescence with increasing solvent polarity. Herein, water-soluble bis(indolium) dyes, synthesized in only one step are reported, that exhibit remarkable 2PA performance, coupled to the ES-SB process, displaying a counterintuitive fluorescence blue shift in polar solvents. The relationship between their chemical structure and the extent of the ES-SB and 2PA properties is investigated via steady-state optical spectroscopies and transient absorption spectroscopy (TAS). The unusual blue shift is ascribed to their dicationic nature, leading to an uneven stabilization of the ground and ES-SB excited states in polar environments due to inefficient excited state solvation and positive charge confinement. These compounds also offer specific mitochondrial staining of living HeLa cells, performing at the level of more complex commercial mitochondria markers. Herein, a novel family of dicationic dyes are introduced with robust 2PA properties and practical use in bioimaging and provide connections between their dication quadrupolar nature, which imparts larger water solubility, 2PA performance, and ES-SB, which improving fluorescence properties and bioimaging microscopy detection and resolution.

1. Introduction

Water-soluble fluorescent organic dyes capable of functioning in biological media have the potential to optically probe and unveil fundamental phenomena occurring in complex cellular processes. In this context, fluorescence microscopy finds an excellent resource on two-photon absorption (2PA), which provides 3D controlled excitation following from its quadratic dependence on the excitation light intensity.[1–4] This highly desired feature is further complemented with reduced tissue photodamage and improved in-depth penetration at the working wavelengths, usually at the NIR region (i.e., 700–1000 nm).[5,6] Thus, different strategies have been proposed for the design of efficient fluorescent 2PA chromophores with applications in biosensing and bioimaging.[7,8]

In recent years, several reports have underlined the tight association between the efficacy of quadrupolar structures to achieve superior 2PA cross-sections (σ_{2PA})

C. Benitez-Martin, F. Najera, E. Perez-Inestrosa
Departamento de Química Orgánica
Universidad de Málaga
Andalucía-Tech Campus Teatinos s/n, Málaga ES-29071, Spain
E-mail: najera@uma.es; inestrosa@uma.es

C. Benitez-Martin, F. Najera, E. Perez-Inestrosa
Instituto de Investigación Biomédica de Málaga y Plataforma en Nanomedicina–IBIMA
Plataforma Bionand
Parque Tecnológico de Andalucía, Málaga ES-29590, Spain

The ORCID identification number(s) for the author(s) of this article can be found under https://doi.org/10.1002/adma.202510730

DOI: 10.1002/adma.202510730

C. Benitez-Martin
Department of Chemistry & Molecular Biology
University of Göthenburg
Goteborg 41390, Sweden

J. M. Marin-Beloqui, J. T. L. Navarrete, J. Casado
Department of Physical Chemistry
University of Málaga
Andalucía-Tech Campus de Teatinos s/n, Málaga ES-29071, Spain
E-mail: casado@uma.es

J. M. Marin-Beloqui, J. Casado, F. Najera, E. Perez-Inestrosa
Materials and Nanotechnology Institute (IMANA)
University of Malaga
Campus de Teatinos s/n, Málaga 29071, Spain

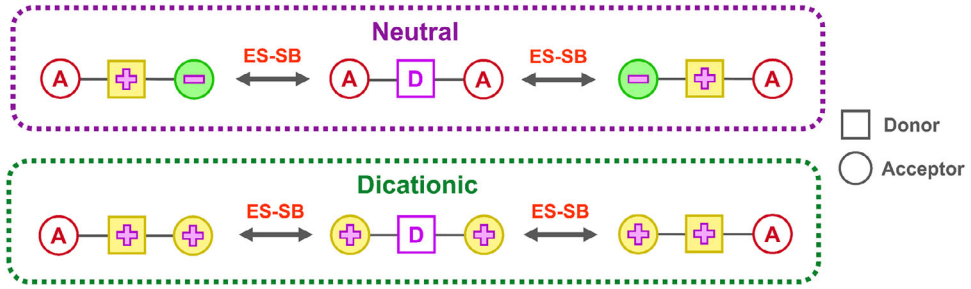

Scheme 1. Valence bond description of the dipole formation in the ES-SB processes in (*top*) conventional neutral dyes, and in (*bottom*) bis(indolium) dication salts proposed as new designs for more efficient bioimaging dyes. D/square: electron donor, A/circle: electron acceptor.

and excited state symmetry breaking (ES-SB).[9,10] ES-SB involves the partial or entire polarization of the S_1 electron density to form a locally uneven distribution toward one of the branches of the molecule (**Scheme 1**). Indeed, ES-SB has been extensively studied in neutral molecules with electron donor-acceptor arrays, and is critically driven by the presence of polar solvents.[11–14] In contrast, the 2PA process in this type of dyes emerges from the coupling of their electronic ground with higher energy lying excited states (typically S_2), whose σ_{2PA} is directly associated with the quadrupolar transition moment upon photoexcitation. Consequently, while 2PA and ES-SB are associated with different transitions, they remain intimately coupled by internal conversion and interconnected through the dipolar/quadrupolar character of their excited state wavefunctions. Designing efficient 2PA chromophores for bioimaging applications thus requires a dual optimization strategy: enhancing the S_1 state for ES-SB, while optimizing simultaneously the S_2 state for a strong 2PA response.[15–17]

The first hallmark for the ES-SB process is a fluorescence red shift with increasing solvent polarity. This bathochromic displacement of the emission serves as an accessible and widely utilized preliminary test, with its application being well-established in the majority of studies on ES-SB with neutral quadrupolar molecules.[14,15,18–20] This shift originates from the reduction of the electronic bandgap in polar solvents as a consequence of a greater stabilization of the excited state, inherently more polar than the ground state in conventional neutral ES-SB systems. However, we report an example where this preliminary test reveals a completely opposite behavior, i.e., a blue shift in emission is detected in more polar solvents. This blue shift usually entails a larger emission efficiency, particularly in more polar solvents, which is beneficial for 2PA-detection with fluorescence methods.[21]

As represented in **Schemes 1** and **2**, we envisaged symmetrical A-π-D-π-A fluorophores that interconnect two cationic electron-acceptor 1,3,3-trimethyl-3*H*-indolium moieties with different electron-donor aromatic cores via vinylene π-bridges. The use of positively charged building blocks as acceptor units, opposite to the most used neutral ones, enhances water solubility of the dyes as well as facilitates their integration into biological media. Water solubility, pivotal for biological applications, is usually pursued by additional and complementary chemical functionalization,[7] which implies adverse problems such as the use of large amounts of solvents, additional purification steps, or complications in scalable methods, etc. Additionally, these indolium moieties impart the desired electron-acceptor character to spark the polarization-mediated ES-SB effect. As the electron-donor, a selection of small π-cores was chosen to modulate the electron-donor character, including those from highly polarizable thiophene and bithiophene to highly luminescent phenyl and biphenyl cores.

The in-depth spectroscopic analysis of these systematically modified derivatives allowed the characterization of their ability to perform 2PA. Furthermore, our studies provided valuable insights into how the so-populated 2PA excited state (S_2) is coupled to its parent vicinal (S_1), which experiences ES-SB at the origin

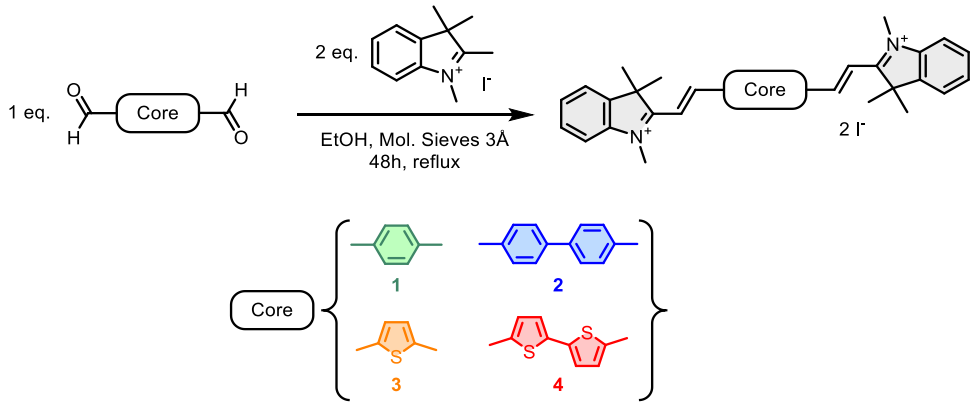

Scheme 2. Preparation of symmetric dicationic bis(indolium) dyes **1**–**4**.

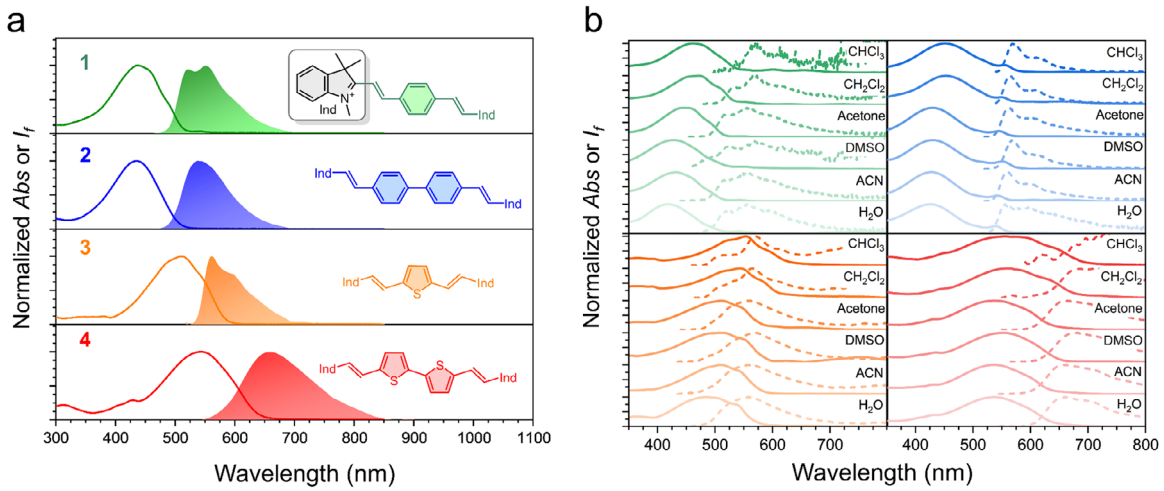

Figure 1. a) Normalized absorption (lines) and fluorescence intensity (solid bands) spectra of compounds **1–4** in acetonitrile (10^{-5} M, air-equilibrated solution). b) Normalized absorption (solid lines) and emission (dashed lines) spectra of compounds **1–4** in a series of different polarity solvents (optically diluted air-equilibrated solution, the increase in solvent polarity is represented by the fading of the respective colors chosen for each dye).

of the luminescence features used for bioimaging. We found out a counterintuitive blue shift in fluorescence when increasing solvent polarity, also observed in other cationic molecules that undergo ES-SB.[9,21–23] This contrasts with conventional 2PA molecules, where the emission is often red-shifted in polar environments such as biological media. This bathochromic shift in neutral conventional dyes comes, however, at the cost of reduced fluorescence efficiency due to enhanced non-radiative pathways related to a decreased bandgap according to the energy gap law.[24] Consequently, our charged derivatives, displaying a blue-shifted emission with increasing polarity, should preserve or even improve their emission performance, with the great benefit for their detection in aqueous solution and biological media.

To confirm the presence of the ES-SB mechanism, we employed transient absorption spectroscopy (TAS)[9,16,22,23,25–29] in combination with the preparation of their truncated counterparts. Then, we compared the excited states of our final molecules with the excited states of their truncated derivatives since they are expected to closely resemble our molecule's ES-SB excited state. Additionally, we examined the relationship between 2PA properties and the ES-SB process, aiding in correlating the efficiency of the ES-SB mechanism and the σ_{2PA}.

Finally, we demonstrated the application of these molecules for bioimaging by incubating them with living cells. Fluorescent microscopy reveals that these 2PA dicationic dyes stain selectively and specifically mitochondria. Mitochondria, often referred to as the cell powerhouses, are central to cellular energy metabolism.[30,31] The mitochondria are also a major source of reactive oxygen species at the subcellular level, which are small but crucial mediators involved in both physiological and pathological processes.[32] Thus, the success of our easy-to-synthesize dyes, which perform at the same level as more complex and costly commercial alternatives, provides a valuable new toolbox to selectively monitor mitochondria, a vital component in cells and life.

2. Results and Discussion

2.1. Synthesis

Compounds **1–4** were synthesized via Knoevenagel-type condensation between commercially available aromatic dicarboxaldehydes and 1,2,3,3-tetramethyl-3*H*-indolium iodide (Scheme 2). More details about the synthesis and characterization (mono- and bidimensional NMR spectra, and mass spectrometry) of these dyes are provided in the Supporting Information.

2.2. Ground State Spectroscopic Characterization

2.2.1. One-Photon (1P) Absorption and Emission

The corresponding 1P absorption and emission spectra are shown in **Figure** 1a, and their key photophysical data are summarized in Table S1 (Supporting Information).

Generally, these dyes are characterized by being strong light absorbers in the visible region (Figure S1, Supporting Information) with almost negligible absorbance at higher energies than that of the main transition. This finding was further corroborated by TD-DFT calculations, which predicted low to negligible oscillator strengths for the transitions in the spectral region below 400 nm (see Supporting Information). As observed, dyes **1** and **2**, endorsed with phenyl-based cores, display blue-shifted absorption maxima compared to their thiophene counterparts **3** and **4**. This red shift in 3 and 4 implies a decreased bandgap when incorporating greater electron-donor thiophene-based cores and indirectly indicates an enhanced donor-acceptor character on these molecules. The introduction of an additional thiophene group in **4** extends the π-conjugated system and provokes a further red shift of its absorption maximum when compared to **3**. This

effect is, however, not observed when comparing **2** versus **1**. Indeed, **2** presents a slightly blue-shifted absorption. Noteworthy, akin trends are found when examining the fluorescence properties of these compounds. The analysis of DFT optimized geometries supports this maximum absorbance band trend (see DFT calculations section in Supporting Information). This increased structural flexibility of **2** explains the reduced electron density overlap and delocalization from the center phenyl group to the bis(indolium) groups, and the subsequent blue-shifted bands (see Supporting Information for a more extended discussion).

Interestingly, the absorbance and fluorescence spectra obtained using different solvents reveal certain changes in position when varying the solvent polarity (Figure 1b). The normalized per photon absorbed emission spectra can be found in the Supporting Information. The absorbance and fluorescence maxima display a blue shift as solvent polarity increases. This is rather unusual, as the emission of conventional 2PA dyes is commonly bathochromically shifted when increasing solvent polarity.[14,15,18–20] This behavior is nevertheless consistent with other examples of charged molecules that undergo ES-SB. In these cases, the blue shift in absorbance is sustained by a larger dipole/quadrupole moment of the ground state in comparison with that of their excited state.[22,23] Fluorescence quantum yields were obtained for our molecules in all the studied solvents (Table S2, Supporting Information), which displayed very low yields, from 0.001 to 0.023, with the highest fluorescence quantum yields found in **3** and **4**.

2.2.2. Multiphotonic 2PA Characterization

The 2PA properties of these compounds were explored via the two-photon induced fluorescence method in the 700–1000 nm range.[3] The low fluorescence quantum yield of our molecules could raise uncertainties in the 2PA characterization. However, it is important to clarify that the relevant figure-of-merit in these analyses is the product of the two-photon cross-section times the fluorescence quantum yield. Therefore, despite the modest fluorescence quantum yields, the large 2PA cross-sections of our compounds (and in particular **4**) enable clear observation of two-photon fluorescence with a high signal-to-noise ratio. The 2P excitation and 2P-induced fluorescence spectra or the studied molecules are represented in **Figure 2** (see also Figure S3, Supporting Information). We chose acetonitrile as the solvent because it is widely used in such studies, facilitating direct comparison with other molecules with indolium as acceptor units in the literature data.[27,33,34]

All molecules display two 2PA bands: i) a very intense band at 700–720 nm with significant σ_{2PA}, and ii) a secondary feature at ≈890 nm exhibiting lower intensity (Figure 2b; Figure S3, Supporting Information). It is important to emphasize that 2PA-induced fluorescence resembles that observed upon one-photon excitation for all cases. This corroborates that emission does not rely on the vertically populated electronic excited state but on the first excited state, which is rapidly populated by $S_2 \rightarrow S_1$ internal conversion following Kasha's rule.[35] Moreover, the biphotonic origin of this emission was further confirmed with the representation of the emission intensity versus the laser power (see Figure S4, Supporting Information). This representation in a double logarithmic plot shows lines with slopes of ≈2 for all molecules, which unequivocally correspond to two-photon processes. Furthermore, the sharp decrease at 700 nm of the 2PA excitation spectra of **3** and **4** helps to rule out the existence of resonance effects (since 1PA and 2PA overlap at ≈700 nm for these two molecules). Importantly, the σ_{2PA} values obtained are comparable to those described for other state-of-the-art related structures (as seen in Tables S4 and S5, Supporting Information).[9,22,23,27–29,36–39]

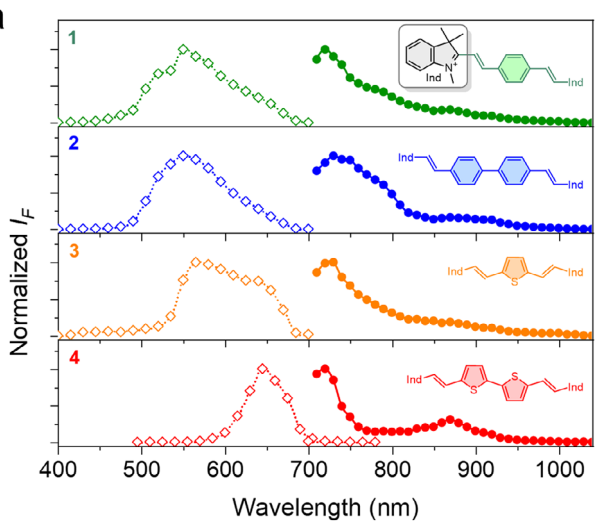

b

Compound	$\lambda_{abs,2P}$ (nm)	σ_{2PA} (GM)
1	700	425
	890	30
2	700	248
	890	30
3	700	510
	890	48
4	720	4443
	890	1510

Figure 2. a) 2P-induced fluorescence (dashed) and 2P excitation (solid) spectra of compounds **1**–**4** in acetonitrile (10^{-5} M, air-equilibrated solution). b) σ_{2PA} at selected wavelengths determined by 2P-excited fluorescence method. The complete spectra are shown in Figure S3 (Supporting Information).

2.3. Quantum Chemical Calculations

To gain more insights into the relationships between one-photon absorption and 2PA, calculations were performed at the CAM-B3LYP/6-311+G(2d,p) level of theory.[40] The solvent was considered by including the polarization continuum model (PCM).[41] Table S3 (Supporting Information) summarizes the most significant data related to the absorption, accurately reproducing the experimental data (differences in all cases were ≤0.1 eV). In line with the 2PA selection rules, the $S_0 \rightarrow S_1$ transition is not active under 2P-excitation conditions.[42–44] Calculations confirm that the $S_0 \rightarrow S_2$ transition, however, appears as the most active for the 2PA process for dyes **1**–**3**. Regarding compound **4**, although the

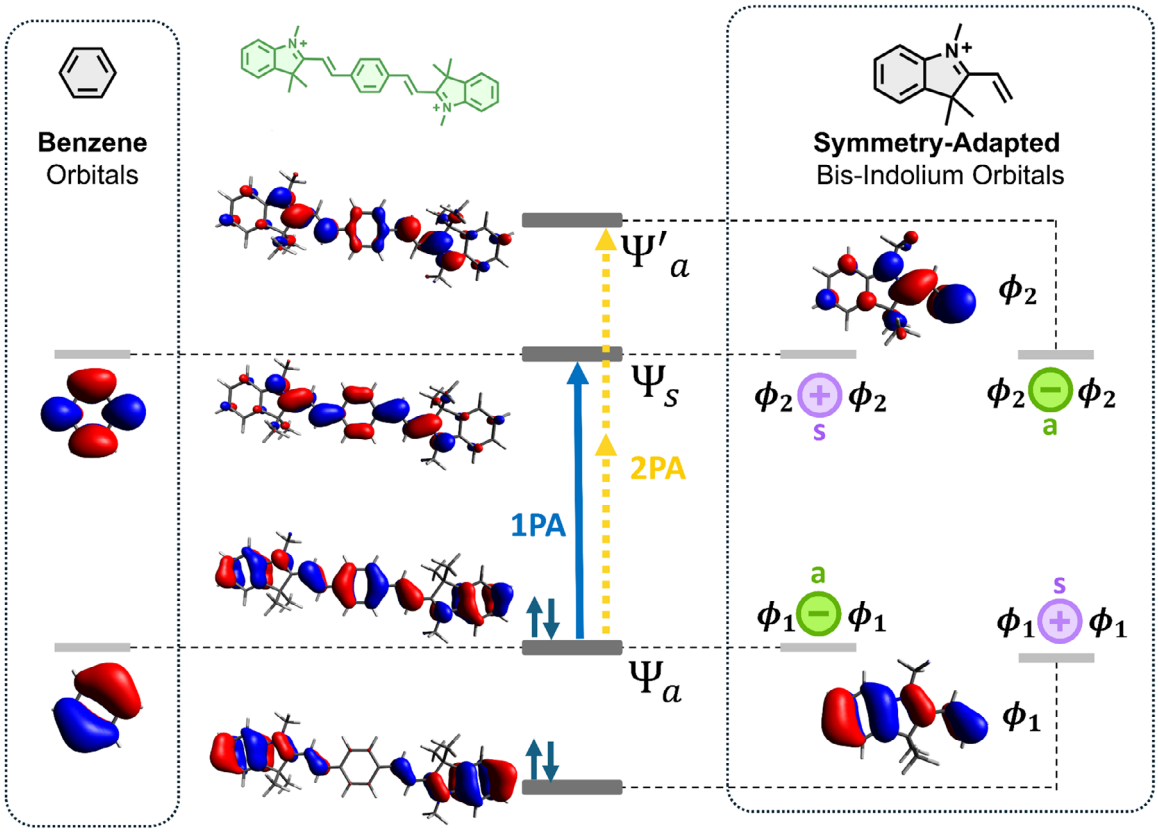

Figure 3. Orbital evolution of **1** (calculated by DFT at the PCM(ACN)/CAM-B3LYP/6-311+G(2d,p) level from the central benzene coupled with the external bis(indolium-vinylene moieties). The symbols *a* and s represent the antisymmetric and symmetric character of the orbitals of the benzene core and of the linear combination of the orbitals of the two bis(indolium)-vinylene peripheral units.

$S_0 \rightarrow S_2$ transition is also 2PA accessible, the most prominent one is the $S_0 \rightarrow S_3$.

The results provided by the calculations about selection rules of the one-photon absorption and 2PA properties can also be explained by a fragmental frontier orbitals approach to the electronic structure of the relevant compounds. For this purpose, wavefunctions of the relevant orbitals of **1** as a representative example are constructed in **Figure 3** by combining the orbitals of the central moiety (benzene in **1**) with symmetry-adapted orbitals derived from the orbital combination of both bis(indolium)-vinylenes. Thereby, the HOMO of **1** emerges as the *antisymmetric* linear combination of the benzene HOMO with the symmetry-adapted orbital (i.e., *antisymmetric* combination) of the bis(indolium)-vinylene HOMOs. Conversely, the LUMO of **1** is produced by a *symmetric* combination of the benzene LUMO with the *symmetric* linear combination of the LUMOs of the two bis(indolium)-vinylene fragments. As a result, the HOMO→LUMO transition, corresponding to the $S_0 \rightarrow S_1$ excitation, is optically one-photon allowed (*g*→*u*, for centrosymmetric molecules) and carries out a strong orbital wavefunction overlap as both HOMO and LUMO delocalize across the entire molecule. This provokes a strong variation of the electric dipolar transition moment, consistent with the TD-DFT calculations discussed in the previous paragraph and in the Supporting Information. Furthermore, the LUMO+1 orbital of **1** is mainly composed of the *antisymmetric* combination of the bis(indolium)-vinylenes LUMOs (though the calculation shows a secondary contribution from the central benzene, which is not captured by our approach). Consequently, the HOMO and LUMO+1 are *antisymmetric* combinations of the fragment orbitals, and the HOMO to LUMO+1 transition, corresponding to the $S_0 \rightarrow S_2$ excitation, will shift electron density from the central benzene toward the external indolium cations. This redistribution results in a symmetric double acceptor←donor→acceptor charge polarization, inducing a significant variation of the electric quadrupolar transition moment. Hence, the preserved symmetry and the change in the electric quadrupolar transition moment along the HOMO→LUMO+1 transition grant this transition as 2PA allowed, opening an excitation route for photonic applications.

2.4. Transient Absorption Characterization

The symmetry of these compounds and their significant σ_{2PA} values lead us to explore the presence of ES-SB. Therefore, we decided to perform femtosecond Transient Absorption Spectroscopy (fs-TAS) to further elucidate the nature of the excited states. The results obtained for fs-TAS characterization of **4**, the molecule with the largest σ_{2PA}, are shown in **Figure 4a**. Further fs-TAS analysis of the other derivatives is included in the Supporting Information.

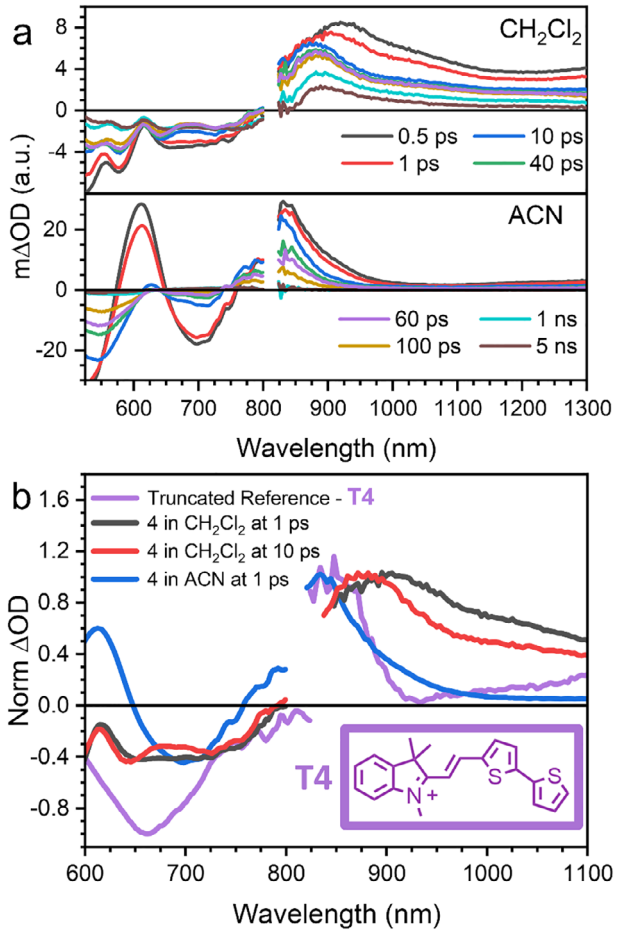

Figure 4. a) fs-TAS for **4** dissolved in (*top*) dichloromethane and (*bottom*) acetonitrile taken at different delay times. b) Comparison of the spectra for **4** in different solvents and timescales with the spectrum of the truncated reference in CH_2Cl_2 (purple). Samples were excited at 500 nm with a power of 0.25 mW. ΔOD stands for differences of optical density.

Exciting compound **4** at 500 nm in dichloromethane induces the rapid development of a positive band centered at 910 nm and extending into the NIR region, as observed in Figure 4a. Concurrently, negative features below 800 nm are observed, attributed to ground-state bleaching (GSB) and stimulated emission (SE) phenomena. Within the first picoseconds, the positive band at 910 nm undergoes a blue shift of ≈40 nm before finally decaying to the ground state with a 2 ns lifetime. Concurrently, the broad, featureless SE band—spanning 650–750 nm and matching the steady-state fluorescence of **4** in dichloromethane (Figure 1b)—shifts from 656 to 650 nm before fully dissipating within 10 ps. In stark contrast, when the solvent is switched to acetonitrile, the TAS results show a single band centered at 830 nm that becomes narrower within the first picosecond and decays with a significantly shorter lifetime of 63 ps. Furthermore, there is a positive band at 600 nm which swiftly decays, matching the scale of the 830 nm band narrowing. This 600 nm feature matches the local maxima of **4** when dissolved in dichloromethane; however, it gets obscured by the GSB in this solvent. Notably, a similar response is observed in water as detailed in Figure S5 (Supporting Information). We performed global analysis on the TA data to identify the species involved upon photoexcitation (Figure S6, Supporting Information). However, it should be noted that this mathematical approach is less reliable when spectral shifts occur. The analysis reveals a rapid transformation within the first picoseconds, where the vertically excited state relaxes into a more stable configuration with lifetimes of 30–60 ps. For compound **4** in dichloromethane, this relaxed state further evolves into long-lived species (i.e., likely triplets, given their large lifetimes). Interestingly, the relative contribution of the vertically excited state (compared to the relaxed state), as estimated from their absorption maxima intensities, decreases with increasing solvent polarity. This interpretation assumes similar excited-state absorptivity across all solvents (i.e., this should be considered with caution).

The solvent-dependent behavior obtained in these TAS results aligns with the ES-SB process in the sense that in a less polar solvent, such as dichloromethane, the molecule gradually evolves toward a non-symmetric electronic distribution, as observed by the time-dependent blue shift. These timescales, where the ES-SB state is achieved in picoseconds, are coherent with other results reported in the literature.[16,20,26,45] Conversely, in the highly polar acetonitrile, the broken symmetry state is rapidly and more effectively stabilized within the time resolution of the measurement.[25,46–48] The charged nature of this excited state is further corroborated by the pronounced reduction in its lifetime with increasing solvent polarity, decreasing from ≈2 ns in dichloromethane to 63 ps in acetonitrile.

Although TAS results strongly suggest the presence of an ES-SB process, to definitively ascribe this phenomenon to an ES-SB event, fs-TAS was conducted on a truncated asymmetric derivative of **4**, containing only one indolium moiety and designated as **T4** (Figure 4b). The synthesis of this compound is provided in Section S1 (Supporting Information). It is reasonable to expect that the spectroscopic response of the ES-SB excited state of **4** would feature similar fingerprints as the TAS response of the truncated analogue, **T4**.[9,22] The TA spectrum of **T4** reveals a positive feature centered at 840 nm, which swiftly decays to the ground state. The striking similarity between the excited-state absorption profile of the truncated **T4** and that of **4** in polar solvents provides compelling evidence that, upon excitation, compound **4** unambiguously locally redistributes its electronic density toward one of the two indolium units via an ES-SB mechanism.

The TAS results for the rest of the compounds (**1**-**3**), along with the comparison with their truncated derivatives, are included in the Supporting Information.This TA data suggested a more efficient ES-SB mechanism in **4** in comparison with the other studied compounds. This difference becomes particularly evident when examining the truncated analogues: **T4** maintains closer excited state absorbance similarity to its complete counterpart, while the other three truncated compounds' excited state absorbance deviates from their symmetric counterparts. Hence, the TAS data revealed a clear correlation between the occurrence of the ES-SB process and the σ_{2PA} values for these molecules. The differences in ES-SB behavior observed between compounds **3** and **4**, compared to **1** and **2**, respectively, underscore the beneficial influence of thiophene

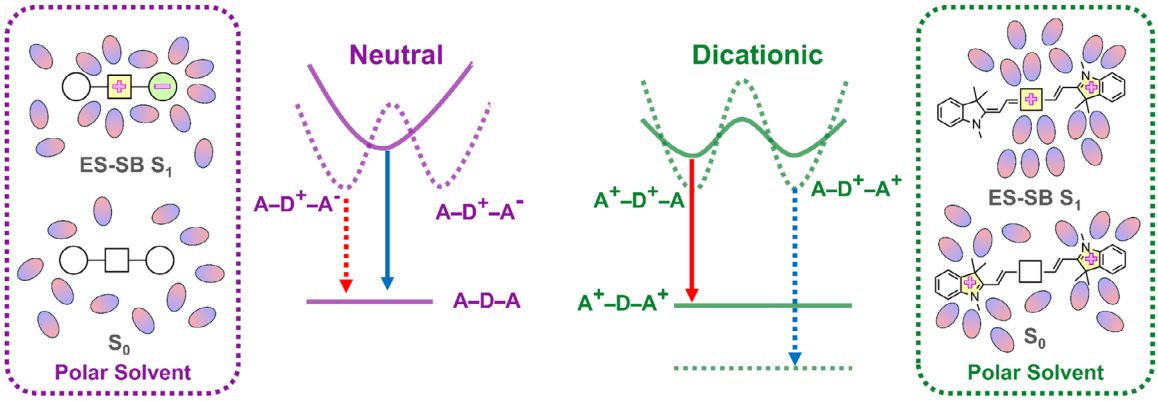

Figure 5. Potential energy surface diagram comparing a conventional neutral ES-SB molecule (left) and our synthesized molecules (right), illustrating the energy level variations in low-polarity (solid) and polar (dashed) solvents. Squares and circles represent the donor and acceptor moieties, respectively.

as a donor group compared to the phenyl group. The enhanced donor ability of thiophene notably promotes ES-SB, leading to larger σ_{2PA} values. However, the largest difference was seen by increasing the donor moiety length, as seen in **4**, which shows the clearest ES-SB, which matches the largest σ_{2PA} value.

2.5. Further Discussion of the Photophysical Characterization

As stated in the introduction, fluorescence solvatochromism is usually described in literature as the first indication of ES-SB. In conventional neutral dyes, excitation leads to a neutral excited state that evolves into a polarized electronic distribution through an ES-SB process. Locally, this ES-SB excited state becomes significantly more polar than the neutral ground state and, therefore, gets largely stabilized by polar solvents, which decreases the optical energy gap, causing a red shift of the fluorescence in polar solvents in comparison with apolar ones. The situation in our dication dyes, however, is different as their ground states are inherently polar. In S_0, the spatially separated indolium cations allow an efficient solvation of the charges by solvent molecules. However, in the ES-SB S_1 state, the smaller spatial separation of the positive charges reduces the efficiency of solvation by the overcrowding presence of solvent molecules in the first sphere of solvation (**Figure 5**). These factors collectively result in a greater stabilization of the S_0 state relative to the SB S_1 one, ultimately increasing the optical gap on going from apolar to polar media. This is the underlying cause of the fluorescence band blue shift observed with increasing solvent polarity.

2.6. Bioimaging Cell Studies with 1–4 in Aqueous Medium

The optical properties of these compounds render them potential candidates for bioimaging applications; their performance within living cells was finally investigated. HeLa cells were first incubated for 2 h with 1 μM solutions of **1–4** in complete medium and then examined by 2P microscopy (more details are included in the Supporting Information). Please note that this concentration was previously demonstrated to be harmless for HeLa cells by cytotoxicity assay (Figure S19, Supporting Information).

The incubation of our dyes with HeLa cells showed two different behaviors (Figure S20, Supporting Information). The fluorescence stemming from **1–3** described a particular filamentous pattern, which strongly suggested mitochondrial accumulation of these derivatives. This situation was somehow expected, as the incorporation of positive charges in lipophilic structures has been demonstrated in other fluorophores as an efficient strategy to achieve selective accumulation within mitochondria.[31,33] On the other hand, **4** displayed a weaker signal, this mostly localized in small, unidentified vesicles. We therefore focused our attention on studying the performance of dyes **1–3** in-depth. The control experiments showed no significant background fluorescence (Figure S21, Supporting Information).

To confirm the mitochondrial distribution of dyes **1–3**, we then conducted colocalization studies with commercial mitochondria trackers: MitoTracker Red CMXRos (**MTR**) or MitoTracker Green FM (**MTG**). The results from these studies are illustrated in **Figure 6**, where **1** and **2** are represented in green and counterstained against **MTR**, colored in red. When looking at the merge of the respective images, all the fluorescence is orange to yellow, resulting from the combination of green and red channels and indicating that the effectiveness of our dye and the commercial one to stain mitochondria is comparable. Pearson Correlation Coefficients (PCCs) with the commercial **MTR** were calculated as 0.80 and 0.78 for **1** and **2**, respectively. These high PCCs values document a good correlation between the fluorescence signals of our dyes and the commercial **MTR** and confirm the ability of these dicationic derivatives to stain mitochondria. A similar readout can be reached when examining compound **3**, depicted in magenta, and counterstained with **MTG**, illustrated in cyan. In this case, the combined signals are colored in blue, and an excellent PCC of 0.82 was obtained.

3. Conclusion

Bis(indolium) dyes are a novel family of compounds with excellent 2PA properties, ideal for fields such as material sciences and biomedicine due to their straightforward synthesis, which allows for fine-tuning their photophysical properties via facile

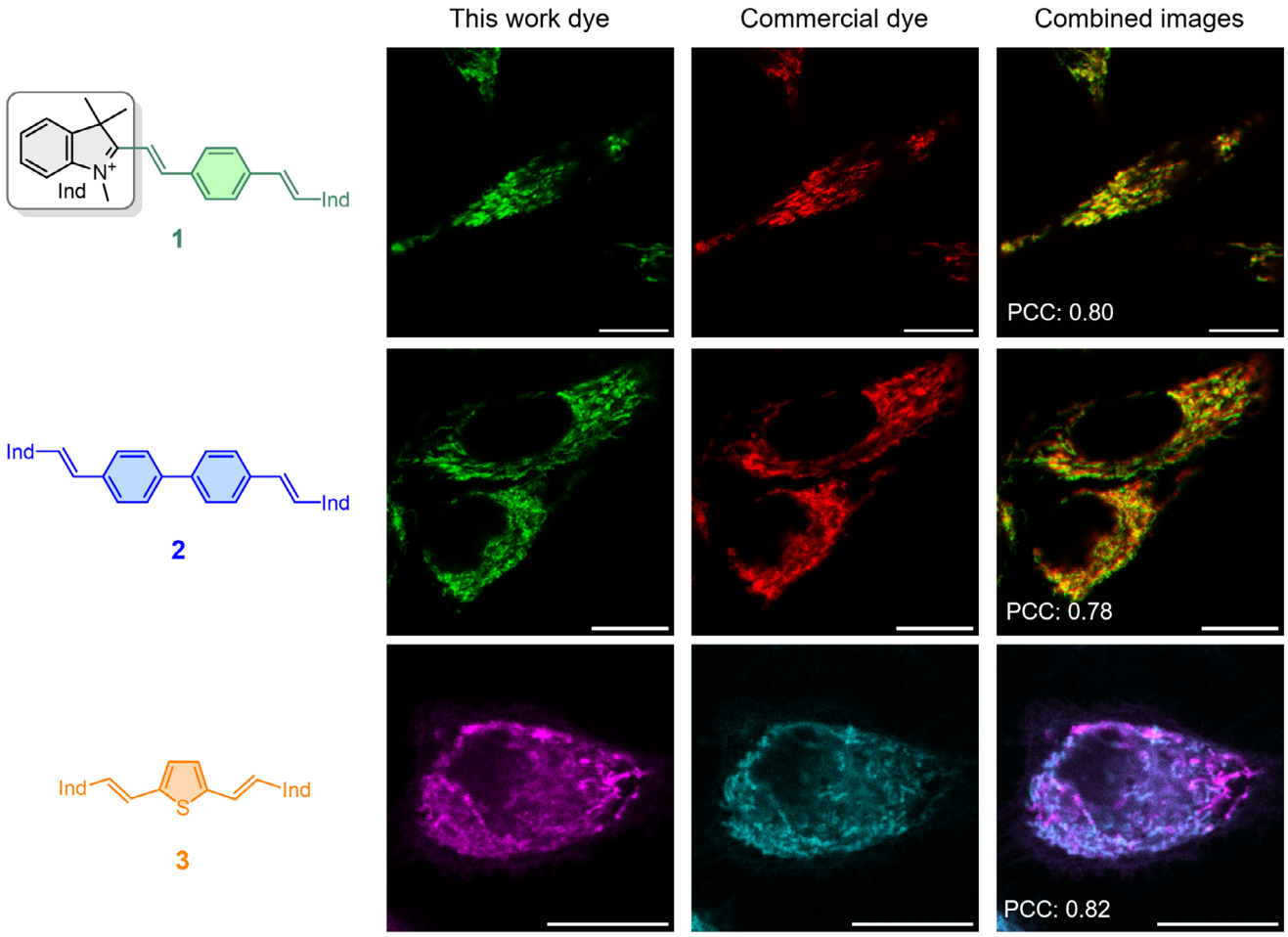

Figure 6. Comparison between **1**–**3** and commercial mitochondria-specific marker within living HeLa cells. The Pearson Correlation Coefficient (PCC) is indicated for each specific case. The following fluorescence channels are shown: **1**→$\lambda_{exc,\ 2P}$ = 700 nm, λ_{em} = 500–520 nm (represented in green), **2**→$\lambda_{exc,\ 2P}$ = 700 nm, λ_{em} = 500–520 nm (represented in green), **3**→$\lambda_{exc,\ 2P}$ = 700 nm, λ_{em} = 600–650 nm (represented in magenta), **MTR**→$\lambda_{exc,\ 1P}$ = 561 nm, λ_{em} = 620–650 nm (represented in red), and **MTG**→$\lambda_{exc,\ 1P}$ = 488 nm, λ_{em} = 500–520 nm. Scale bars: 15 µm.

structural modifications. Their fluorescence revealed an unusual blue shift in emission maxima with increasing solvent polarity, contrasting with the red shifts typically reported for conventional neutral ES-SB molecules. Still, the fs-TAS characterization confirmed the occurrence of the ES-SB process in these dyes. This unique behavior arises from the dicationic nature of their ground state, which is more effectively stabilized by polar solvents compared to their ES-SB state. In the ES-SB state, the closer proximity of charges reduces solvent stabilization efficiency, increasing the fluorescence energy gap and causing the observed blue shift. Incorporating a thiophene group as donor induced clearer ES-SB compared to a phenyl group. In addition, extending the donor length significantly enhanced the ES-SB process: compounds with a single donor repeating unit exhibited inefficient ES-SB, and, correspondingly, lower σ_{2PA}. Bioimaging studies in living HeLa cells demonstrated that compounds **1–3** function as mitochondria-specific stains, enabling high-quality imaging via two-photon microscopy. These dyes performed comparably to commercial mitochondrial markers, despite their much simpler design. This work delivers a novel family of water-soluble, easily synthesized 2PA molecules, along with key structural design strategies to enhance ES-SB and maximize 2PA performance.

Supporting Information

Supporting Information is available from the Wiley Online Library or from the author.

Acknowledgements

C.B.-M. and J.M.M.-B. contributed equally to this work. The authors acknowledged the Spanish Ministry of Science, Innovation and Universities (E.P.I. and F.N. for project PID2022-136705NB-I00 and J.C. and J.M.M.-B. for projects PID2024-157601NB-100 and RED2022-134939-T –Red de Fotovoltaica) and the Junta de Andalucía (EPI for project FQM-017 and J.C. for project PROYEXCEL-0328). C.B.M. thanks the Spanish Ministry of Universities for a FPU predoctoral contract (FPU16/ 02516). J.M.M.-B. wants to acknowledge the Spanish University Ministry and the European Union for its Maria Zambrano fellowship with NextGen-Eu funding and the University of Malaga. The authors gratefully acknowledged the ICTS "NANBIOSIS" facilities, more specifically the U28 Unit of the Andalusian Centre

for Nanomedicine & Biotechnology (BIONAND), where the 2PA characterization had been carried out. The authors also thank the Research Central Services (SCAI) of the University of Málaga for access to the EVI, EEL, and MENL to perform ground state and transient spectroscopic characterisation. Finally, the authors acknowledge the computer resources, technical assistance, and expertise provided by the SCBI (Supercomputing and Bioinformatics) Centre of the University of Málaga.

Conflict of Interest

The authors declare no conflict of interest.

Data Availability Statement

The data that support the findings of this study are available from the corresponding author upon reasonable request.

Keywords

bioimaging, excited state symmetry breaking, fluorescence, mitochondria, two-photon absorption

Received: June 6, 2025
Revised: September 2, 2025
Published online:

[1] M. Albota, D. Beljonne, J. L. Brédas, J. E. Ehrlich, J. Y. Fu, A. A. Heikal, S. E. Hess, T. Kogej, M. D. Levin, S. R. Marder, D. McCord-Maughon, J. W. Perry, H. Röckel, M. Rumi, G. Subramaniam, W. W. Webb, X. L. Wu, C. Xu, *Science* **1998**, *281*, 1653.
[2] G. S. He, L. S. Tan, Q. Zheng, P. N. Prasad, *Chem. Rev.* **2008**, *108*, 1245.
[3] F. Terenziani, C. Katan, E. Badaeva, S. Tretiak, M. Blanchara-Desce, *Adv. Mater.* **2008**, *20*, 4641.
[4] M. Pawlicki, H. A. Collins, R. G. Denning, H. L. Anderson, *Angew. Chem., Int. Ed.* **2009**, *48*, 3244.
[5] W. Denk, J. H. Strickler, W. W. Webb, *Science* **1990**, *248*, 73.
[6] P. A. Shaw, E. Forsyth, F. Haseeb, S. Yang, M. Bradley, M. Klausen, *Front. Chem.* **2022**, *10*, 921354.
[7] C. S. Lim, B. R. Cho, *Tetrahedron* **2015**, *71*, 8219.
[8] H. W. Liu, Y. Liu, P. Wang, X. B. Zhang, *Methods Appl. Fluoresc.* **2017**, *5*, 012003.
[9] A. Cesaretti, A. Spalletti, F. Elisei, P. Foggi, R. Germani, C. G. Fortuna, B. Carlotti, *Phys. Chem. Chem. Phys.* **2021**, *23*, 16739.
[10] G. Ramakrishna, T. Goodson, *J. Phys. Chem. A* **2007**, *111*, 993.
[11] B. Dereka, A. Rosspeintner, Z. Li, R. Liska, E. Vauthey, *J. Am. Chem. Soc.* **2016**, *138*, 4643.
[12] B. Dereka, A. Rosspeintner, M. Krzeszewski, D. T. Gryko, E. Vauthey, *Angew. Chem., Int. Ed.* **2016**, *55*, 15624.
[13] B. Dereka, E. Vauthey, *J. Phys. Chem. Lett.* **2017**, *8*, 3927.
[14] Ł. G. Łukasiewicz, M. Rammo, C. Stark, M. Krzeszewski, D. Jacquemin, A. Rebane, D. T. Gryko, *ChemPhotoChem* **2020**, *4*, 508.
[15] B. Dereka, A. Rosspeintner, R. Stężycki, C. Ruckebusch, D. T. Gryko, E. Vauthey, *J. Phys. Chem. Lett.* **2017**, *8*, 6029.
[16] Z. Szakács, E. Vauthey, *J. Phys. Chem. Lett.* **2021**, *12*, 4067.
[17] Z. Szakács, F. Glöcklhofer, F. Plasser, E. Vauthey, *Phys. Chem. Chem. Phys.* **2021**, *23*, 15150.
[18] X. Xu, S. Gunasekaran, S. Renken, L. Ripani, D. Schollmeyer, W. Kim, M. Marcaccio, A. Musser, A. Narita, *Adv. Sci.* **2022**, *9*, 2200004.
[19] H. Song, H. Zhao, Y. Guo, A. M. Philip, Q. Guo, M. Hariharan, A. Xia, *J. Phys. Chem. C* **2020**, *124*, 237.
[20] X. Niu, Z. Kuang, M. Planells, Y. Guo, N. Robertson, A. Xia, *Phys. Chem. Chem. Phys.* **2020**, *22*, 15743.
[21] A. B. Ryabitsky, A. D. Kachkovski, O. V. Przhonska, *J. Mol. Struct.: THEOCHEM* **2007**, *802*, 75.
[22] B. Carlotti, E. Benassi, C. G. Fortuna, V. Barone, A. Spalletti, F. Elisei, *ChemPhysChem* **2016**, *17*, 136.
[23] B. Carlotti, E. Benassi, A. Spalletti, C. G. Fortuna, F. Elisei, V. Barone, *Phys. Chem. Chem. Phys.* **2014**, *16*, 13984.
[24] R. Englman, J. Jortner, *Mol. Phys.* **1970**, *18*, 145.
[25] J. H. Golden, L. Estergreen, T. Porter, A. C. Tadle, D. M. R. Sylvinson, J. W. Facendola, C. P. Kubiak, S. E. Bradforth, M. E. Thompson, *ACS Appl. Energy Mater.* **2018**, *1*, 1083.
[26] I. Papadopoulos, M. J. Álvaro-Martins, D. Molina, P. M. McCosker, P. A. Keller, T. Clark, Á. Sastre-Santos, D. M. Guldi, *Adv. Energy Mater.* **2020**, *10*, 2001496.
[27] Y. Feng, P. J. Das, R. M. Young, P. J. Brown, J. E. Hornick, J. A. Weber, J. S. W. Seale, C. L. Stern, M. R. Wasielewski, J. F. Stoddart, *J. Am. Chem. Soc.* **2022**, *144*, 16841.
[28] L. Mencaroni, C. Bonaccorso, V. Botti, B. Carlotti, G. Consiglio, F. Elisei, C. G. Fortuna, A. Spalletti, A. Cesaretti, *Dyes Pigm.* **2021**, *194*, 109620.
[29] F. Ricci, B. Carlotti, B. Keller, C. Bonaccorso, C. G. Fortuna, T. Goodson, F. Elisei, A. Spalletti, *J. Phys. Chem. C* **2017**, *121*, 3987.
[30] K. Shen, C. L. Pender, R. Bar-Ziv, H. Zhang, K. Wickham, E. Willey, J. Durieux, Q. Ahmad, A. Dillin, *Annu. Rev. Cell Dev. Biol.* **2022**, *38*, 179.
[31] H. M. Kim, B. R. Cho, *Chem. Rev.* **2015**, *115*, 5014.
[32] M. I. Anik, N. Mahmud, A. A. l. Masud, M. I. Khan, M. N. Islam, S. Uddin, M. K. Hossain, *ACS Appl. Bio Mater.* **2022**, *5*, 4028.
[33] C. Benitez-Martin, F. Najera, E. Perez-Inestrosa, *Sens. Actuat. B Chem.* **2025**, *423*, 136862.
[34] C. Benitez-Martin, J. A. Guadix, J. R. Pearson, F. Najera, J. M. Perez-Pomares, E. Perez-Inestrosa, *Sens. Actuat. B Chem.* **2019**, *284*, 744.
[35] M. Kasha, *Discuss. Faraday Soc.* **1950**, *9*, 14.
[36] C. Sissa, F. Terenziani, A. Painelli, A. Abbotto, L. Bellotto, C. Marinzi, E. Garbin, C. Ferrante, R. Bozio, *J. Phys. Chem. B* **2010**, *114*, 882.
[37] M. Auvray, F. Bolze, D. Naud-Martin, M. Poulain, M. Bossuat, G. Clavier, F. Mahuteau-Betzer, *Chem. Eur. J.* **2022**, *28*, 202104378.
[38] M. Auvray, F. Bolze, G. Clavier, F. Mahuteau-Betzer, *Dyes Pigm.* **2021**, *187*, 109083.
[39] S. Griesbeck, Z. Zhang, M. Gutmann, T. Lühmann, R. M. Edkins, G. Clermont, A. N. Lazar, M. Haehnel, K. Edkins, A. Eichhorn, M. Blanchard-Desce, L. Meinel, T. B. Marder, *Chem. Eur. J.* **2016**, *22*, 14701.
[40] T. Yanai, D. P. Tew, N. C. Handy, *Chem. Phys. Lett.* **2004**, *393*, 51.
[41] J. Tomasi, B. Mennucci, R. Cammi, *Chem. Rev.* **2005**, *105*, 2999.
[42] M. Marín, J. P. Telo, D. Collado, F. Nájera, E. Pérez-Inestrosa, U. Pischel, *Chem. Eur. J.* **2018**, *24*, 2929.
[43] I. Torres-Moya, C. Benitez-Martin, B. Donoso, C. Tardío, R. Martín, J. R. Carrillo, Á. Díaz-Ortiz, F. Najera, P. Prieto, E. Perez-Inestrosa, *Chem. Eur. J.* **2019**, *25*, 15572.
[44] C. Benitez-Martin, B. Donoso, I. Torres-Moya, J. Herrera, Á. Díaz-Ortiz, F. Najera, P. Prieto, E. Perez-Inestrosa, *Dyes Pigm.* **2022**, *200*, 110149.
[45] P. Verma, M. Tasior, P. Roy, S. R. Meech, D. T. Gryko, E. Vauthey, *Phys. Chem. Chem. Phys.* **2023**, *25*, 22689.
[46] Y. Wu, R. M. Young, M. Frasconi, S. T. Schneebeli, P. Spenst, D. M. Gardner, K. E. Brown, F. Würthner, J. F. Stoddart, M. R. Wasielewski, *J. Am. Chem. Soc.* **2015**, *137*, 13236.
[47] A. N. Bartynski, M. Gruber, S. Das, S. Rangan, S. Mollinger, C. Trinh, S. E. Bradforth, K. Vandewal, A. Salleo, R. A. Bartynski, W. Bruetting, M. E. Thompson, *J. Am. Chem. Soc.* **2015**, *137*, 5397.
[48] N. Mataga, H. Yao, T. Okada, W. Rettig, *J. Phys. Chem.* **1989**, *93*, 3383.